

Internal Solitons in the Andaman Sea

A. R. Osborne and T. L. Burch

Internal waves occur within subsurface layers of marine waters that are stratified because of temperature and salinity variations. Disturbances created within the ocean give rise to these waves, which represent a significant mechanism for the transport of momentum and energy within the ocean. Historically, oceanographers have given care-

Sea in October 1976. The program was designed to simultaneously measure internal waves and the associated response of the drillship *Discoverer 534*, which was drilling at that time in more than 1030 m of water. The analysis of these data is presented here; the problem of drillship response to internal waves has been reported elsewhere (1, 2).

Summary. The solitary wave is a localized hydrodynamic phenomenon that can occur because of a balance between nonlinear cohesive and linear dispersive forces in a fluid. It has been shown theoretically, and observed experimentally, that some solitary waves have properties analogous to those of elementary particles, and the waves have therefore been named solitons. During a measurement program in the Andaman Sea near northern Sumatra, large-amplitude, long internal waves were observed with associated surface waves called tide rips. Using theoretical results from the physics of nonlinear waves, it is shown that the internal waves are solitons and their interactions with surface waves are described.

ful attention to internal waves and their side effects, for they can significantly influence oceanic current measurements, undersea navigation, antisubmarine warfare operations, and even the feeding habits of marine animals.

In late 1975 and early 1976, internal wave currents as high as 1.8 meters per second were observed during a 4-month measurement program and subsequent drilling operations conducted by Exxon in 600 to 1100 meters of water in the Andaman Sea, offshore Thailand (1). As a result of this study, Exxon concluded that knowledge of internal wave behavior would be necessary for the design of future deepwater offshore production facilities. Internal wave data were also obtained during an ensuing 4-day measurement program in the southern Andaman

In this article we discuss a theoretical framework for the interpretation of data described by internal solitons—solitary waves which, by definition, retain their shape and speed after colliding with each other. We present a preliminary analysis of the Andaman Sea data within this framework and show that the data corroborate the occurrence in nature of solitons. Finally, we discuss the interaction of internal solitons with surface waves in light of our observations of an unusual surface wave phenomenon previously referred to as the “tide rip.”

To understand the behavior of internal solitary waves and solitons, it is helpful to understand surface solitary waves—waves that travel on the surface of the water rather than beneath it. To this end, we first present some historical evidence

for surface solitary waves and further discuss evidence for interactions between internal solitary waves and surface waves.

Historical Setting

The study of wave phenomena in physics is undergoing dramatic changes as a result of the discovery of solitons (3). These localized nonlinear waves have a number of unusual properties compared to linear waves, which have formed the basis for most physical theories of wave phenomena. Historically, solitary waves were thought to self-destruct when they collide with each other. Since the discovery of solitons, efforts have been made to determine whether certain solitary waves behave as solitons. Mathematical and numerical techniques have been devised to test whether solitary wave solutions of a particular system can survive a collision with each other—that is, whether they retain their shape and speed after the collision and therefore deserve the designation soliton. Examples of physical systems that have been shown to have soliton solutions are water waves, ion-acoustic waves and magnetohydrodynamic waves in a plasma, pressure waves in liquid-gas bubble mixtures, propagation of sound waves through a crystal lattice, and phonon packets in low-temperature nonlinear crystals (4).

Apparently, the first documented observation of a solitary wave was made by John Scott Russell (5, p. 319) in the 19th century:

I was observing the motion of a boat which was rapidly drawn along a narrow channel by a pair of horses, when the boat suddenly stopped—not so the mass of water in the channel which it had put in motion; it accumulated round the prow of the vessel in a state of violent agitation, then suddenly leaving it behind, rolled forward with great velocity, assuming the form of a large solitary elevation, a rounded, smooth and well-defined heap of water, which continued its course along the channel apparently without change of form or diminution of speed. I followed it on horseback, and overtook it still rolling on

A. R. Osborne is a research physicist at Exxon Production Research Co., Houston, Texas 77001. T. L. Burch is an oceanographer and program manager at EG & G Environmental Consultants, Waltham, Massachusetts 02154.

at a rate of some eight or nine miles an hour, preserving its figure some thirty feet long and a foot to a foot and a half in height. Its height gradually diminished and after a chase of one or two miles I lost it in the windings of the channel. Such, in the month of August, 1834, was my first chance interview with that singular and beautiful phenomenon.

Scott Russell went on to make rather precise, well-controlled observations of solitary waves. A model differential equation describing solitary wave behavior was not developed until 1895, when Korteweg and deVries (6) approximated the Navier-Stokes equations for small finite-amplitude waves in a shallow channel. The Korteweg-deVries (K-dV) equation (7) will be described in the following section.

Another historical precursor that is relevant to our data interpretation and to the interaction of surface and internal waves is given in Maury (8). This is a description by Horsburgh (made sometime before 1861) of a "tide rip":

In the entrance of the Malacca Straits, near the Nicobar and Acheen Islands, and between them and Junkseylon, there are often very strong riplings, particularly in the southwest monsoon; these are alarming to persons unacquainted, for the broken water makes a great noise when the ship is passing through the riplings in the night. In most places riplings are thought to be produced by strong currents, but here they are frequently seen when there is no perceptible current . . . so as to produce an error in the course and distance sailed, yet the surface of the water is impelled forward by some undiscovered cause. The riplings are seen in calm weather approaching from a distance, and in the night their noise is heard a considerable time before they come near. They beat against the sides of a ship with great violence, and pass on, the spray sometimes coming on deck; and a small boat could not always resist the turbulence of these remarkable riplings.

Because the observation above occurred in relatively deep water, the phenomena described cannot be the result of a classical tide rip. Tide rips are due to strong tidal currents flowing over bars and through inlets which oppose the propagation of surface waves, creating regions of short, choppy, breaking waves. For this reason, we will simply refer to the strange waves first observed by Horsburgh as "rips" throughout this article.

Perry and Schimke (9) made observations of rips north of Sumatra from the U.S. Coast and Geodetic Survey ship *Pioneer* in 1964. They described

. . . distinct zones of whitecaps ranging from 200 to 800 m in width and stretching from horizon to horizon (approximately 30 km) in a north-south direction . . . in the Andaman Sea north of Sumatra. At least five of these zones, with a spacing of about 3200 m between each zone, were observed. The observed zones or

bands of choppy water had short, steep, randomly oriented waves with heights of about 0.3 to 0.6 m. Each band stood out distinctly in an otherwise undisturbed sea. A 4 m/sec NNW wind and a surface water temperature of 29°C were observed, but neither changed significantly as the ship crossed the bands of choppy water.

Using a mechanical bathythermograph, Perry and Schimke obtained several profiles of water temperature from the surface down to 250 m during the rip passages and were able to associate the rips with internal waves as large as 80 m. Phillips (10) has reviewed Perry and Schimke's rip observations in light of interactions between long internal waves and surface waves.

Similar surface phenomena were reported in the Indian Ocean (11) and in the Bay of Bengal and adjacent waters (9), where they were variously described as current rips, tide rips, lines of demarcation, disturbed water, and rippled water.

Solitons

The observations of solitary waves by Scott Russell and the subsequent theoretical description by Korteweg and de Vries represented the extent of physical understanding of solitary waves at the beginning of this century. For nearly 70 years thereafter, the solitary wave was considered a relatively unimportant curiosity in the field of nonlinear wave theory. It was generally thought that the collision of two solitary waves would result in a strong nonlinear interaction and ultimately end in their destruction (4). Then in 1965 Zabusky and Kruskal (3) reported on a computer experiment in which they simulated the K-dV equation for the collision of two solitary waves. The results of the simulation were surprising: the waves retained their shapes and propagation velocities after the collision. Because of the somewhat elementary particle-like behavior of these waves, Zabusky and Kruskal coined the word "soliton" to describe them.

We first briefly recount the solitary wave theory of Korteweg and deVries. The K-dV equation for the propagation of surface solitary waves is given by

$$\eta_t + c_0\eta_x + \alpha\eta\eta_x + \gamma\eta_{xxx} = 0 \quad (1)$$

$$c_0 = \sqrt{gh}$$

$$\alpha = 3c_0/2h \quad (2)$$

$$\gamma = c_0h^2/6$$

Here $\eta(x,t)$ is the amplitude of the solitary wave as a function of horizontal displacement x down the channel and of time t ; h is the water depth; g is the ac-

celeration due to gravity; and c_0 is the phase speed of the associated linear wave. The subscripts in Eq. 1 refer to partial derivatives with respect to x or t . We will see later that not only surface solitary waves but also internal solitary waves may be described by the K-dV equation. The key to understanding this equation lies in the competition between the nonlinear term ($\alpha\eta\eta_x$) and the dispersive term ($\gamma\eta_{xxx}$). Under certain conditions these terms balance, and the result is a stable configuration called the solitary wave which is a special solution of Eq. 1 and has the analytical form

$$\eta(x,t) = \eta_0 \text{sech}^2[(x - ct)/L] \quad (3)$$

where η_0 is the maximum amplitude of the solitary wave, $c = c_0(1 + \eta_0/2h)$ is the phase speed of the wave, and $L = \sqrt{4h^3/3\eta_0}$ is its characteristic length. A surface solitary wave is shown in Fig. 1 and clearly may be described as a bump on the water, in strong contrast to the appearance of the linear "sine" wave.

In 1967, Gardner *et al.* (12) presented an analytical solution of the initial value problem governed by the K-dV evolution equation and analytically predicted the behavior of the soliton. Given an arbitrary initial wave form $\eta(x,0)$, how does it evolve thereafter in time according to the K-dV equation? The character of the Gardner *et al.* solution is illustrated in Fig. 2. A sufficiently localized initial wave form $\eta(x,0)$ (12-14) will evolve into one or more solitons and a dispersive tail or wave train as $t \rightarrow \infty$. With normalizations for amplitude, horizontal coordinate, and time

$$u = 3\eta/2h$$

$$r = (x - c_0t)/h \quad (4)$$

$$\tau = c_0t/6h$$

the K-dV equation may be written in the convenient form

$$\mu_\tau + 6uu_\tau + u_{\tau\tau\tau} = 0 \quad (5)$$

The essential results of Gardner *et al.* may then be easily summarized as a set of rules that govern the behavior of long, nonlinear waves (solitons) described by the K-dV equation for a channel of constant depth and constant breadth (14). We emphasize the importance of these rules in the interpretation of soliton signals in experimental data.

1) Soliton amplitudes must be positive definite, $u(r,t) \geq 0$, and are given by the dimensionless solution

$$u(r) = 2A \text{sech}^2[\sqrt{A}(r - 4A\tau)] \quad (6)$$

where the amplitude $2A$ is found from Eq. 8 below.

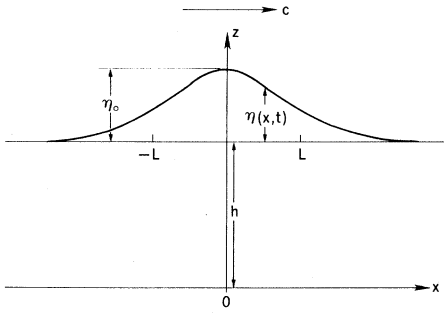


Fig. 1. Surface solitary wave with amplitude η_0 moving to the right with phase speed c in water of depth h .

2) The dimensional soliton phase speed exceeds the phase speed of the associated linear wave c_0 by an amount proportional to its amplitude

$$c = c_0(1 + 2A/3) \quad (7)$$

3) Since larger solitons travel faster, they evolve into ordered groups, the largest leading the rest (note Fig. 2).

4) No acceptable initial wave form can evolve into two solitons of the same phase speed; that is, two identical solitons cannot be created by a single initial wave form.

5) Interacting solitons experience at most a phase shift, advancing the faster and retarding the slower. Their phase speeds and shapes remain unaltered after they collide with each other.

6) If the area under the initial wave form is positive (and sufficiently local), at least one soliton emerges.

7) If the initial wave form is everywhere negative, no soliton emerges; only the tail or train of dispersive linear waves is formed.

8) The nondimensional amplitude of the largest soliton (assuming the initial wave form is small) is

$$A = \frac{1}{2} \left[\int_{-\infty}^{\infty} u(r,0) dr \right]^2 \geq 0 \quad (8)$$

9) The number of solitons N that emerge may be found from the Schrödinger equation, where the potential well is defined by the dimensionless initial wave form $u(r,0)$

$$\begin{aligned} d^2\phi/dr^2 + u(r,0)\phi + 0 \\ \phi(r_0) = 1 \\ d\phi(r_0)/dr = 0 \end{aligned} \quad (9)$$

The number of zeros of ϕ is the number of solitons that evolve from the initial wave form.

10) The amplitudes A for each member of a soliton packet may be written in renormalized form (15)

$$\bar{A}_n = [(N - n)/(N - 1)]^2 \quad (10)$$

where n is the number of a particular soliton in a packet ($n = 1$ corresponds to the first and largest soliton, $n = 2$ to the next largest, and so on). Thus the renormalized amplitude of the first soliton is unity and each succeeding soliton is smaller according to Eq. 10.

11) Since the individual solitons evolve with independent amplitudes and phase speeds, the separation distances between solitons in a packet are a direct measure of the propagation distance back to the source. This provides a means of estimating the location of the initial wave form.

Internal Solitons

The characteristic behavior of internal solitons depends on the ratio of the water depth to the soliton scale length $\lambda = 2L$. The three regimes that may be encountered are (i) very deep ($h/\lambda \gg 1$), (ii) very shallow ($h/\lambda \ll 1$), and (iii) intermediate ($h/\lambda \sim 1$). The deepwater case is described by the Benjamin-Ono (B-O) equation (16, 17), the shallow-water case is governed by the K-dV equation, and the intermediate-depth case has been investigated by Joseph (18), Kubota *et al.* (19), and Chen and Lee (20). We are not concerned here with effects related to the deep and intermediate cases, primarily because the theories are incomplete and it is not well understood how waves traveling from deep to shallow water make the transition from the B-O regime to the K-dV regime (20). Because our measurement program was conducted in water about half a scale length deep ($h/\lambda \sim 0.4 \sim 0.6$), we feel that the data may be described to a reasonable order of approximation by the K-dV equation, and thus a detailed investigation of this equation for a two-layer fluid is warranted. We will allude to the possible effects of intermediate and deep water in our comparisons with the data.

In a two-layer fluid, the dimensional form of the K-dV equation is given by Eq. 1, where $\eta(x,t)$ is now the interface displacement between the two fluids as shown in Fig. 3 (21). The upper layer is assumed to have depth h_1 and density ρ_1 ; in the lower layer the respective quantities are h_2 and ρ_2 . For the constant coefficients of Eq. 1, we have approximately

$$c_0 \approx [g(\Delta\rho/\rho)h_1/(1+r)]^{1/2} \quad (11)$$

$$\alpha \approx -(3c_0/2)[(1-r)/h_1] \quad (12)$$

$$\gamma \approx c_0h_1h_2/6 \quad (13)$$

These approximate expressions were obtained by assuming $\rho \approx \rho_1 \approx \rho_2$, which is

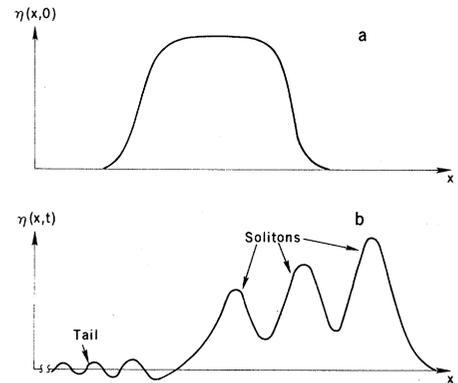


Fig. 2. A sufficiently localized initial wave form (a) evolves into solitons and a dispersive linear wave train or tail in the far field (b).

true in the ocean, where the small density differences are due primarily to temperature and salinity variations. Here $\Delta\rho = \rho_2 - \rho_1$ and $r = h_1/h_2$.

The internal soliton solution to Eq. 1 is

$$\eta(x,t) = -\eta_0 \text{sech}^2[(x - ct)/L] \quad (14)$$

where we have assumed that the upper layer is thinner than the lower layer. This results in a downward displacement of the fluid interface, as indicated by the minus sign before η_0 in Eq. 14. The soliton phase speed is

$$c = c_0(1 - \eta_0\alpha/3c_0) \quad (15)$$

and the scale length is

$$L = (-12\gamma/\eta_0\alpha)^{1/2} \quad (16)$$

The horizontal velocities of the water particles of the soliton in the upper layer are given by

$$u_2(x,t) = (c_0\eta_0/h_1) \text{sech}^2[(x - ct)/L] \quad (17)$$

and in the lower layer by

$$u_1(x,t) = -(c_0\eta_0/h_2) \text{sech}^2[(x - ct)/L] \quad (18)$$

Note that the amplitudes of the horizontal velocities in both layers do not decay with depth, but that the velocities in the lower layer are opposite in direction to those in the upper layer. The vertical velocities do decay with depth but they are not relevant to our data analysis.

Because we are concerned with the case $h_1 < h_2$, the internal soliton is a wave of depression, as pointed out in regard to Eq. 14. Thus, we shall be concerned with modifying items 1, 6, and 7 in our summary of the solution of Gardner *et al.* in order to address internal soliton behavior. When $h_1 > h_2$, negative (downward displaced) internal solitons may emerge from an initial wave form only when its area is negative (average downward displacement of the thermocline). No solitons emerge if the initial

wave form is everywhere positive (upward displacement of the thermocline).

According to Phillips (22), the total internal wave energy per unit crest length is approximately

$$E_T = (\rho_2 - \rho_1)g\bar{\eta}^2 \quad (19)$$

Using Eq. 16, we find

$$\bar{\eta}^2 = \int_{-L}^L \eta^2(x,t)dx = \frac{4}{3} \eta_0^2 L \quad (20)$$

Hence an estimate of the total energy per unit crest length is

$$E_T = \frac{4}{3} (\rho_2 - \rho_1)g\eta_0^2 L \quad (21)$$

These results were derived by assuming equipartition of kinetic and potential energy, which is exact for linear waves and can be shown to be a good approximation for solitary waves.

When a single solitary wave propagates from deep water into shallow water—say from the deep ocean onto the continental shelf—the initial wave may evolve into one or more rank-ordered solitons, a process called soliton fission. Theoretically, this is equivalent to assuming that the solitary wave may be placed directly on the shelf and then allowed to evolve according to the Gardner *et al.* solution. Using the form of the deep-ocean solitary wave developed by Joseph (18), Djordjevic and Redekopp (21) derived a fission law appropriate for determining the number of K-dV internal solitons N appearing on the shelf in a two-layer fluid

$$N \leq 1 + \left[\frac{(32/3)(h_1/h_{2s})(1 - h_1/h_{2s})}{\eta_0/h_1} \right]^{1/2} \ln[(6/\pi)(\eta_0/h_1)(h_{2\infty}/h_1)] \quad (22)$$

Here h_{2s} is the lower-layer thickness on the shelf and $h_{2\infty}$ is the lower-layer thickness in deep water.

Thus, rank-ordered internal solitons may occur by (i) evolution from the initial wave form over a constant water depth, or (ii) fission from an initially stable solitary wave that moves over decreasing water depth into shallow water.

Andaman Sea Internal Wave Data

The 4-month measurement program conducted by Exxon in the southern Andaman Sea was needed to determine the severity of the local current environment before drilling operations could begin. Our goal was to assess the potential impact of these currents on the drilling riser—the pipe connecting the drilling ves-

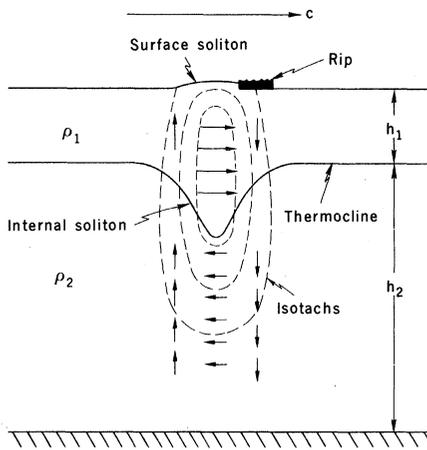


Fig. 3. An internal soliton in a two-layer fluid of finite depth is a wave of depression when $h_1 < h_2$. Dashed lines are lines of constant water particle speed (isotachs); the arrows indicate the magnitude and direction of the water particles. A small surface soliton of amplitude $\sim (\rho_2 - \rho_1)\eta_0$ accompanies the internal soliton (35). The approximate location of the surface rips, as observed in our Andaman Sea measurements, is also shown.

sel to the ocean floor. The preliminary measurement program established the existence of large internal waves in the area, with currents as high as 1.8 m/sec. However, the time resolution coded into the instruments used in the program was rather long, and although this allowed us to measure for an extended period of time, we were unable to determine the detailed structure of the waves.

After these preliminary measurements, we decided to conduct a program with improved time resolution to examine the internal waves in detail while simultaneously measuring the response of a drillship to the wave kinematics. In October 1976, Exxon Production Research Company contracted EG & G Environmental Consultants to conduct an internal wave measurement program in the southern Andaman Sea in 1093 m of water, 7 km west of the drillship *Discoverer 534* at 6°53'N, 97°04'W (see Fig. 4). Current meters (EG & G model CT/3) were placed on a taut subsurface mooring at approximate depths below the ocean surface of 53, 87, 116, 164, and 254 m. These electromagnetic, digitally recording instruments measure water temperature in addition to vector components of horizontal current velocity. In addition, Savonius rotor current meters (EG & G model 102) were located at depths beneath the surface of 121, 437, 635, 895, and 1001 m.

All the instruments were set to record nearly continuously, which limited the total recording capacity to 4 days. From the previous measurement program in

this area, we knew that the internal waves arrived in packets of about five or six waves. The packets were spaced about 12 hours and 26 minutes apart and occurred most noticeably near the twice-monthly spring tides for periods up to 1 week. Thus, we had some confidence that a mooring could be deployed at a time when the internal waves were active. In addition to the moored instrumentation, expendable bathythermograph (XBT) casts were made during periods of internal wave activity. These devices consist of a weighted thermistor, which falls at a prescribed rate through the water column and sends temperature signals to a recording device through a wire of small diameter. Conductivity, temperature, and depth (CTD) casts had previously allowed us to describe the temperature-salinity curve for the region, and thus allowed computation of the spatial and temporal variation of the water density directly from the XBT measurements. Shipboard observations were also used to establish air and surface water temperature, wind speed, cloud cover, ship position, and surface wave height.

Through the cooperation of the National Aeronautics and Space Administration and the National Oceanic and Atmospheric Administration, it was possible to use the LANDSAT and NIMBUS satellites, respectively, for simultaneous observation of the sea surface during our in situ measurements. This was done because the results of Apel *et al.* (23) had shown that internal waves may occasionally be recorded on satellite images because their presence alters the reflectivity of surface waves. We had also received reports of visual observations of surface rips from the drilling vessel and hoped that satellite photography would provide information about the spatial scale of the rips and ultimately of the internal waves. Unfortunately, we were not successful in obtaining satellite photographs during the 4 days of measurements, primarily because of local cloud cover.

We have, however, found more than 40 photographs of the Andaman Sea surface in LANDSAT files (five showing internal waves with crests as long as 150 km and wavelengths as great as 15 km), and Apel (24) has discussed a photograph of the Andaman Sea taken during the Apollo-Soyuz mission. This photograph (see cover) shows three packets of internal waves, two moving from the northwest and one from the southwest. Figure 4 shows the boundary of this photograph projected onto a map of the An-

daman Sea; also shown are the internal wave traces. Apparently (based on this single photograph) there are at least two distinct sources for these internal waves—one somewhere in the Andaman Islands and the other near the southernmost of the Nicobar Islands or northern Sumatra. Since Apel (24) suggests a tidal origin and we later present evidence for the tidal generation of our measured waves, we infer that regions of shallow water near these islands may be source candidates. The blackened areas inside the 200-m contour in Fig. 4 are possible locations of potential source regions near these islands.

To show why we believe the internal waves in the Andaman Sea may be observed from satellite orbit, we include Fig. 5, a sequence of photographs taken on board the survey vessel during the passage of a rip band associated with an internal soliton. Observable in the distance in Fig. 5a is a long band of breaking waves about 1.8 m high approaching from due west. In Fig. 5, b and c, the rip continues to approach. In Fig. 5d the rip band reaches the survey vessel with 1.8-m waves. This condition persisted for several minutes until the trailing edge of the rip passed by (Fig. 5, e to g) and the wave heights quickly dropped to less than 0.1 m. The surface of the Andaman Sea had the appearance of a millpond. Several minutes later another rip approached. The entire process was repeated at approximately 40-minute intervals during the next 4 hours. We observed six distinct rips, each approximately 600 to 1200 m wide. Each rip accompanied an internal soliton, as will be shown below.

While there is no direct proof that the rip phenomenon is the same effect observable on the satellite photographs (we do not have sea surface observations simultaneous with the satellite photographs), the simplest conclusion is that the rips are the long parallel bands so readily observed in the satellite photographs.

Figure 6 shows the result of an XBT cast taken when large internal waves were not present. The temperature structure at this time of year was quite stable. A well-mixed surface layer extends to about 60 m; the temperature then drops from 28° to 12°C at a depth of 200 m and continues to drop to about 8°C at 1000 m. This temperature structure represents a significant density stratification with depth.

Figure 7 shows the thermistor temperature measurements for the first internal wave packet observed during our pro-

gram. Concentrating on the temperature variations that occurred at a depth of 164 m, we note a random, background, small-amplitude internal wave field punctuated by large-amplitude temperature increases, which are positive-definite, rank-ordered signals beginning at 2 hours 12 minutes into the record. The wave amplitudes can be determined approximately by converting the temperature signal to amplitude units, using the temperature gradient from Fig. 6. The first temperature increase in Fig. 7 is 5.2°C, corresponding to a 60-m internal wave. Each succeeding wave is smaller than its predecessor. The pattern is simi-

lar to that in Fig. 2 and suggests a soliton interpretation of the data. The difference between the rank ordering observed in these data and that in Fig. 2 can be ascribed to the fact that the horizontal coordinate in Fig. 2 is space, while in the data of Fig. 7 the coordinate is time. In Fig. 7, time advances to the right while the space coordinate increases to the left. Therefore, in terms of the space coordinate, the leftmost soliton of Fig. 7 is the largest and leads the packet, which is consistent with Fig. 2 and with the theory of Gardner *et al.* The data obtained during the 4-day measurement program show that passages of similar packets oc-

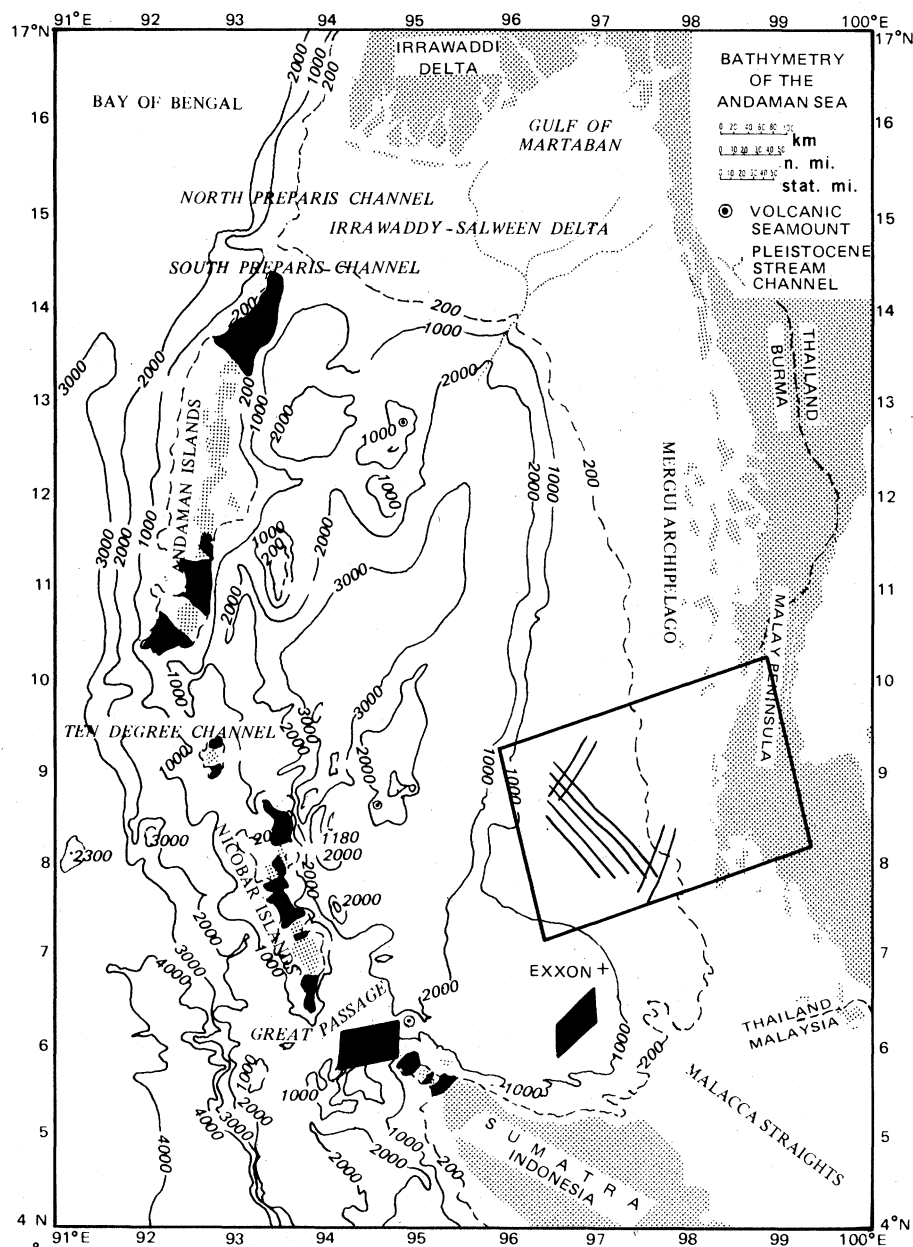


Fig. 4. Map of the Andaman Sea showing the major bathymetric features, the location (indicated by the box) of the satellite photograph (25) on the cover, and the location of the observed internal waves. Potential source regions are shown as blackened areas near the Andaman Islands, the Nicobar Islands, and northern Sumatra. The blackened parallelograms are locations of surface rip observations ("zones of whitecaps") by Perry and Schimke (9).

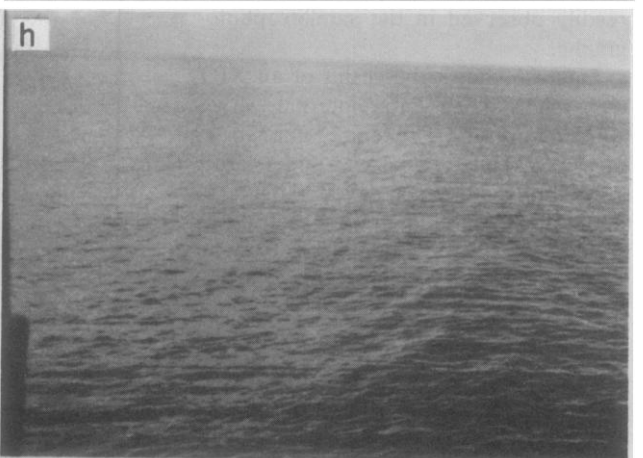
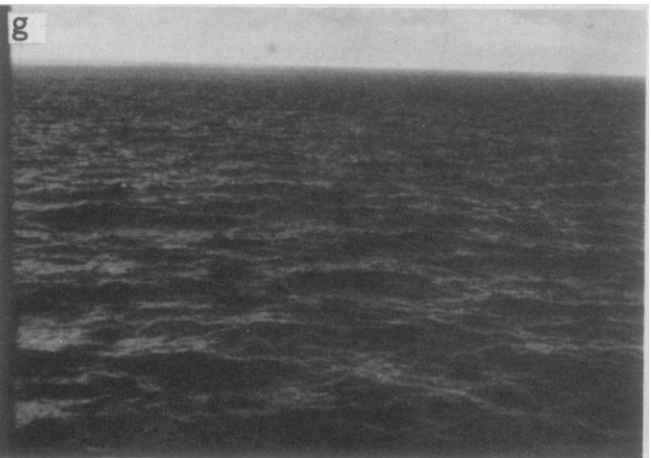
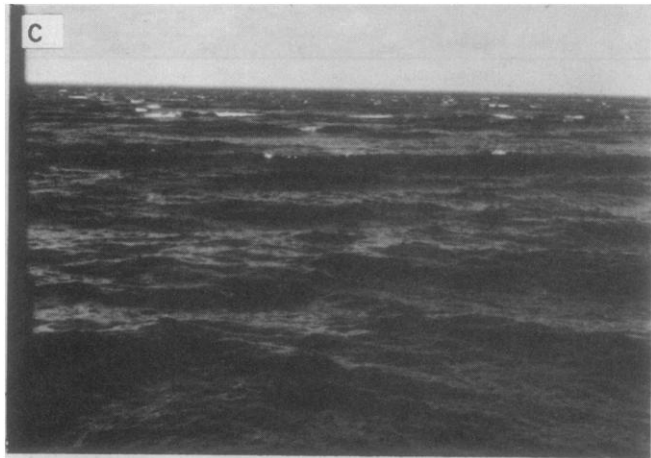
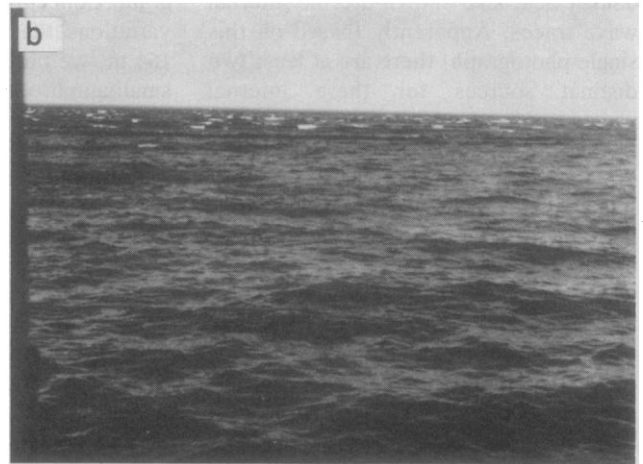
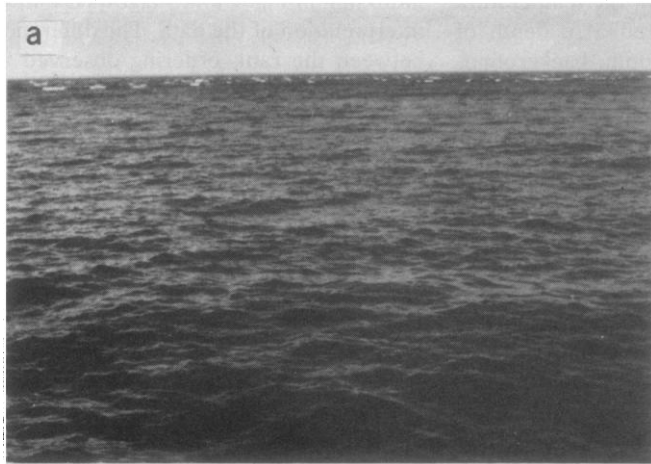


Fig. 5 (facing page). Sequence of photographs of the Andaman Sea surface taken as a rip band approached from the west at a speed of 2.2 m/sec and passed the survey vessel on 27 October 1976 at 10:15 local time (Greenwich mean time + 7 hours). The air temperature was 30°C and the winds were calm during the sequence; (a) 10:15, the rip was seen in the distance, stretching from one horizon to the other, as a well-defined line of breaking waves. The background sea state preceding the rip was ~ 0.6 m and approached from the west; (b) 10:16, the rip continued to approach in background waves of ~ 0.6 m; (c) 10:17, the rip had just arrived at the vessel with wave heights of ~ 1.8 m; (d) 10:19, the survey vessel was tossed about in the 1.8-m waves of the rip band; (e) 10:22, the rearward edge of the rip was visible in 1.8-m waves; (f) 10:23, the rearward edge of the rip receded as the waves dropped to 1.3 m; (g) 10:25, the wave amplitudes dropped to 0.6 m; (h) 10:32, the rip had completely passed as the waves dropped to ripples of ~ 0.1 m.

curred on the average, every 12 hours 26 minutes, which is the semidiurnal tidal period. This indicates that the wave packets are linked in some way to the semidiurnal tide.

The measured eastward components of water particle velocity, obtained simultaneously with the temperature records discussed above, are shown in Fig. 8 as a function of time and depth. Because the eastward component is within 5° of the propagation direction of the internal waves, these velocities are virtually aligned with the wave direction. First, note that the records at the various depths have a nonzero mean due to the presence of an internal tide with maximum particle speeds of about 30 cm/sec. The presence of the internal solitons is evident, although they do not appear rank-ordered unless the tidal signal is removed. The particle velocities for depths of 164 m and above show an eastward enhancement in the flow, while for 437

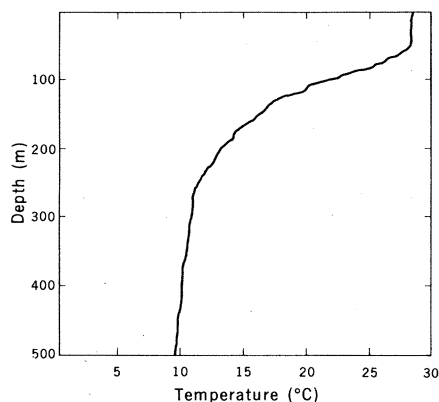


Fig. 6. Typical quiescent temperature structure at the measurement site in the Andaman Sea.

m and below the solitons cause flow enhancements in a westerly direction.

For a preliminary interpretation of these velocity data, we note that the horizontal velocities for a two-layer model are given by Eqs. 17 and 18, where the minus sign before the amplitude in Eq. 18 predicts flow reversal in the lower layer. The ratio of the maximum horizontal velocity in the upper layer to that in the lower layer is h_2/h_1 . Using $h_1 = 230$ m [obtained from the Benney model (25), which takes into account the general stratification found at the measurement site] and $h_2 = 863$ m, we find $h_2/h_1 = 3.75$. The maximum particle velocities for the first wave (amplitude ~ 60 m) at 87 and 1001 m were 55 and 15 cm/sec, respectively. Thus, the measured ratio for this single event is 3.67, which agrees well with the theoretical value. For the same wave, we find from Eq. 11 that $c_0 = 2.14$ m/sec. Hence the theory predicts a maximum velocity in the upper layer of $c_0 \eta_0 / h_1 = 55.8$ cm/sec and in the lower layer of $c_0 \eta_0 / h_2 = 14.9$ cm/sec, both of which agree well with the data. We emphasize here not the accuracy of the two-layer model (we obtained better agreement with the general stratification model), but the facts that (i) there is no particle velocity decay below 600 m, as evidenced by the measured velocities at the lower three current meters, and (ii) the ratio of measured particle speeds in the upper and lower layers (u_1/u_2) is close to the ratio of the depths of the two layers (h_2/h_1). These observations are predicted by the K-dV equation (but are not predicted by the deepwater B-O theory or any of the theories for intermediate depth), and we therefore feel justified in interpreting our results in light of the K-dV equation.

In Fig. 9 we show the results of several XBT casts (every 90 seconds) recorded during the passage of a 60-m internal soliton. Shown as a function of depth are the isotherm contours, which indicate a wave of depression. The time axis increases to the right while the wave advances to the left. The surface rip is on the leading edge of the soliton, a result that we observed consistently for all of the measured waves.

Figure 10 shows the rank ordering of the solitons measured by thermistor at a depth of 116 m. Six soliton packets were observed with an average of nearly five solitons per packet. The amplitude of the first soliton in each packet was normalized to unity, so that decreasing amplitude with increasing soliton number indicates the appropriate rank-ordered behavior. The error bar in Fig. 10, repre-

sents the magnitude of the background internal wave field (viewed as noise), is based on temperature measurements during the "quiet" time between the passage of the soliton packets. Thus, the amplitude of a single wave is considered to be uncertain by an amount equal to

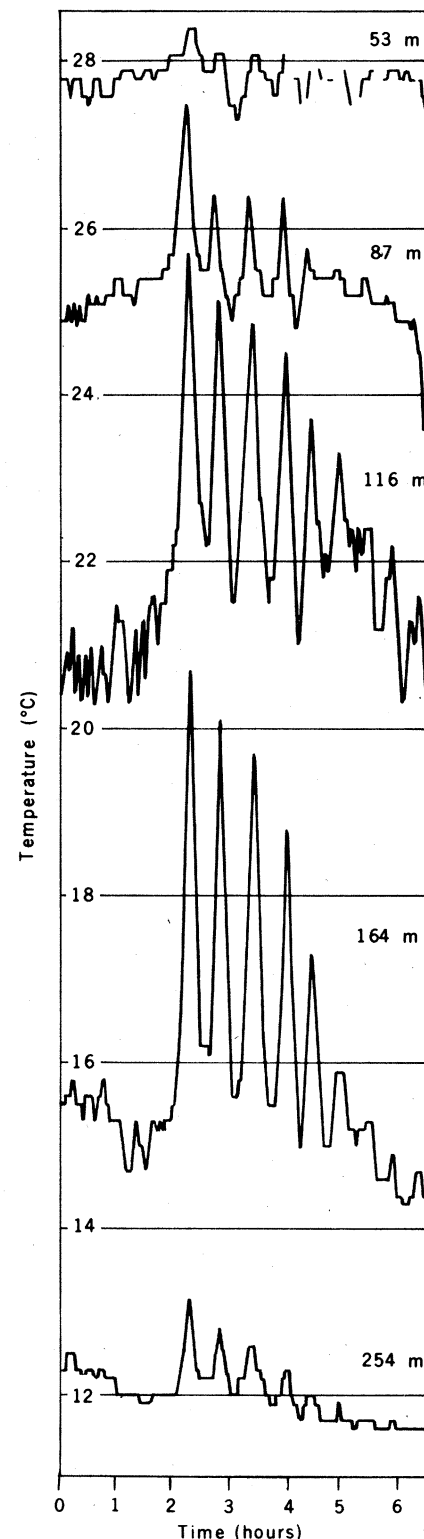


Fig. 7. Temperature signals of internal solitons recorded at several depths on 24 October 1976 beginning at 19:30 local time.

the error bar length. Also shown in Fig. 10 are the curves for normalized amplitude that would result if the number of solitons to evolve was $N = 10, 15,$ and $30,$ as computed from Eq. 10. These curves are predicted by the theory of

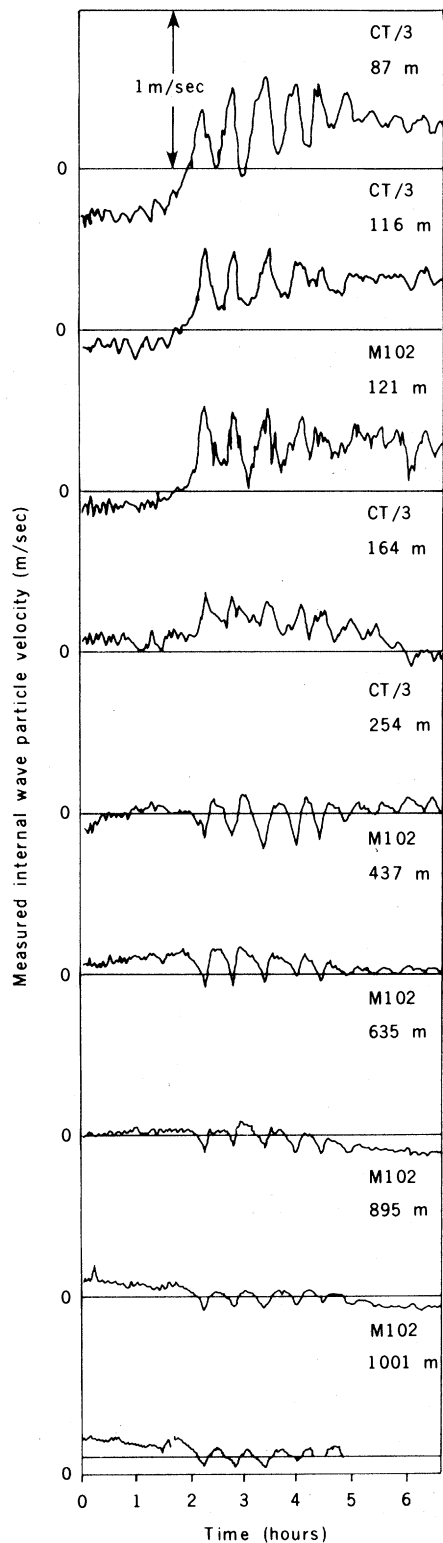


Fig. 8. Eastward particle velocity signals of internal solitons superimposed on an internal tide recorded at several depths on 24 October 1976 beginning at 19:30 local time.

Gardner *et al.*, which assumes that the solitons evolve in a channel of constant breadth and constant depth, with no dissipation. Variations in these parameters could flatten the curves (decrease their slope) for the normalized amplitudes (because they affect the larger leading solitons more than the smaller trailing solitons). Thus we could conjecture that N must be greater than actually observed in order to obtain better agreement with the data. In this article we do not correct for the effects of variable bathymetry, radial spreading, or dissipation. We note, however, that the $N = 15$ curve gives reasonable agreement with the centroid of the amplitudes shown in Fig. 10.

Discussion

In assessing the generation, propagation, and dissipation of internal solitons in the Andaman Sea, we rely on our knowledge of internal wave behavior based on the K-dV equation, taking into account other physical effects that may cause deviations from one-dimensional K-dV behavior. We feel that our overall view of this problem is qualitatively accurate and is also relevant to previous measurement programs that have detected internal solitary waves (26, 27) and to other in situ measurements that have been interpreted in terms of internal solitons (28).

Because the measurements indicate a connection with the semidiurnal tide and the source region must lie to the west of the measurement site, the Nicobar Island chain and northern Sumatra are likely candidates for potential source regions. Applying rule 11 from our summary of the Gardner *et al.* results, we find that the distance from our measurement site to the source is on the order of 300 km, which is consistent with the approximate location of these candidate source regions (we estimated the mean water depth as 1400 m and neglected radial spreading and energy dissipation). Figure 4 shows shallow-water areas near these locations where tidal flow over uneven bathymetry might result in an initial wave form that could evolve into a rank-ordered soliton packet. We note that the average spring tide at Galathea Bay, Great Nicobar Island ($6^{\circ}47'N, 93^{\circ}51'E$), is 1.4 m.

Lee and Beardsley (29) and Maxworthy (30), although not completely in agreement, establish that a "sufficiently localized" wave form can develop from the effects of current flow over uneven bathymetry. Maxworthy's results indi-

cate the likelihood of a lee wave forming to the west of a ridge during westward tidal flow out of the Andaman Sea. On reversal of the tidal flow, the lee wave ultimately propagates over the ridge and develops into the warm trough discussed by Lee and Beardsley. A plausible inference is that the "initial" wave form (the remnant of Maxworthy's lee wave) develops to the east of one or more of the shallow-water areas near the Nicobar Islands and that it is a depression of the thermocline (a warm trough), as this is the only way, theoretically, for internal solitons to arise when the upper layer is thinner than the lower. An initial elevation (a cold dome) will evolve only into a dispersive wave train with no solitons. Because the scale of the sources is small compared to the areal extent of the waves on the satellite photographs, we view the initial wave form as a localized source that immediately begins to propagate and evolves into solitons while undergoing radial spreading, encountering variable topography, and slowly losing energy through dissipation.

The simple one-dimensional, constant-depth, constant-width channel model for the K-dV equation may be modified to

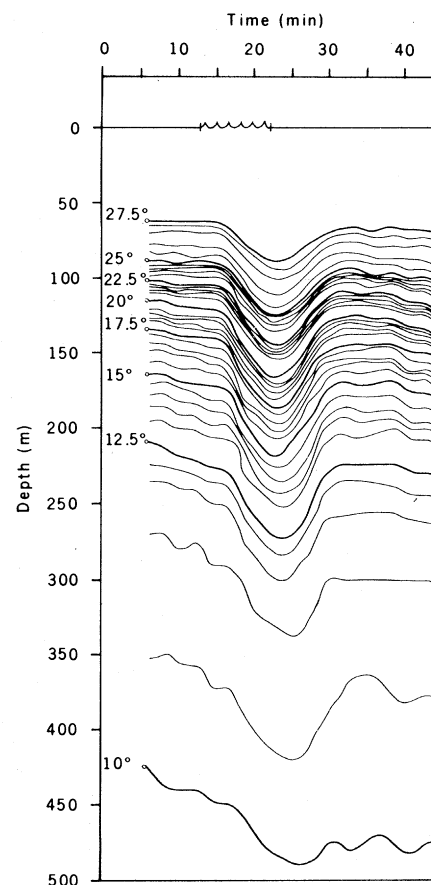


Fig. 9. Isotherm contours of an internal soliton obtained from XBT casts on 25 October 1976 beginning at 8:40 local time.

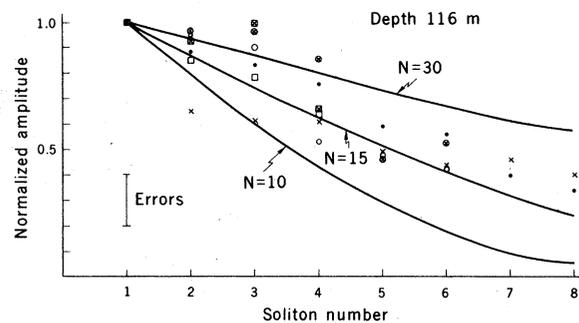
include dissipation effects (28), variable topography and channel width (31, 32), and radial spreading (33, 34). Unfortunately, the results of Gardner *et al.* no longer strictly apply and numerical models for these complex cases must be developed in order to obtain quantitative results. However, the effects on certain predictions of the Gardner *et al.* theory may be discussed qualitatively. For example, radial spreading, dissipation, and increasing water depth will reduce the amplitudes of the larger leading solitons relative to the smaller trailing solitons; these effects will ultimately lead to less rapid decay of soliton amplitude from the front of the packet to the back than predicted by Eq. 10. At present, however, we cannot determine the relative importance of radial spreading, dissipation, and variable topography on our data.

Another mechanism for internal soliton production in the Andaman Sea is the fission process. Because of the extremely varied topography of the Andaman Basin, especially just to the east of the Andaman and Nicobar Islands, the initial warm trough developed in a shallow-water source region might immediately propagate into water depths greater than, say, 3000 m and hence enter the deepwater B-O regime. Such a wave might undergo fission when propagating onto the eastern shelf of the Andaman Sea. Using Eq. 22 for $h_1 = 230$ m, $h_2 = 3000$ m, and $\eta_0 = 70$ m, six or seven solitons are predicted to evolve by the fission process. This is close to the average number of solitons that we observed, and thus fission is a possible means of soliton production in this area.

On the basis of our measurements alone, it is not possible to tell which of the two soliton production modes is more likely in the Andaman Sea. If the warm trough produced in the source region traverses a relatively constant water depth, the Gardner *et al.* solution seems most likely. However, if the warm trough first propagates into deep water and then onto the shelf, the fission process may be the preferred mechanism.

From the satellite photographs and our observations, we can estimate the energy in a typical internal soliton packet from Eq. 21. For a packet of six waves, with leading crest length ~ 100 km, we obtain $\sim 10^{14}$ joules. Thus, an internal soliton encountering the shoreline west of Thailand could dissipate power (per kilometer of crest length) at the rate of 2000 megawatts during the time $\tau = L/c \sim 10$ minutes. However, the duration of such events is rather short and the quiet period between them is long, so there ap-

Fig. 10. Normalized soliton amplitudes for six soliton packets obtained from temperatures measured 116 m below the surface. The error bar indicates the approximate uncertainty in amplitude due to the presence of the background random internal wave field, which is viewed as noise in the present experiment. The different symbols correspond to the six observed packets.



pears to be little likelihood of ever using this energy for practical purposes.

In regard to our observations of surface rips, Phillips (10) pointed out that the "zones of whitecaps" observed by Perry and Schimke (9) might be due to the interaction of surface waves and long, large-amplitude internal waves. Phillips's arguments led to the conclusion that the internal wave orbital velocities sweep the surface wave energy from regions of flow divergence and accumulate it in regions of flow convergence. We established that the internal waves in the Andaman Sea have characteristics of long, large-amplitude internal solitons and that the rips always lie above the leading edge of the solitons, which is a region of flow convergence (see Fig. 3). The resonance condition considered by Phillips occurs when the internal wave phase speed c equals the group velocity of the surface waves c_g , which requires that the surface wavelength be substantially less than the scale length of the internal waves. For the sequence of surface waves shown in Fig. 5 the associated measured internal wave speed was 2.2 m/sec. Assuming that the surface waves were in resonance with the internal soliton and that the surface background waves may be described by a Pierson-Moskowitz spectrum, we estimate the zero crossing period to be ~ 3 seconds and the significant wave height to be ~ 0.6 m. These results are consistent with our visual observations of the surface waves and we conclude that the surface rips are accounted for by the Phillips theory.

The following are several conclusions based on the Andaman Sea data that are consistent with a soliton interpretation:

1) A random, small-amplitude, background internal wave field is punctuated by occasional large-amplitude depressions of the thermocline, which we interpret as internal solitary waves.

2) Internal solitary waves occur in packets of rank-ordered waves, the largest leading the rest. We infer that the waves are internal solitons and that they

evolved either from an initial wave form (over approximately constant water depth) or by the fission process (over variable water depth).

3) Packets occur every 12 hours 26 minutes, indicating a tidal origin for the internal solitons.

4) Likely source regions for the internal solitons are shallow-water areas near northern Sumatra or the southernmost of the Nicobar Islands, where the average spring tidal range is ~ 1.4 m.

5) The initial disturbance in the source region must lead to a depression of the thermocline, as this is the only way internal solitons can be created when the upper layer is thinner than the lower.

6) Measured particle velocities at a given depth tend not to reverse in time, supporting the internal soliton interpretation.

7) Based on satellite photography, the crest lengths of the internal solitons may be as much as 150 km and the separation distance between solitons in a packet as much as 15 km.

8) Internal solitons interact strongly with surface waves, resulting in surface rips (short, choppy, breaking waves), which extend from horizon to horizon and are about 1 km wide.

References and Notes

1. A. R. Osborne, T. L. Burch, R. I. Scarlet, *J. Pet. Technol.* **30**, 1497 (1978).
2. R. A. Warriner and D. H. Shumway, paper presented at the Annual Fall Technical Conference and Exhibition of the Society of Petroleum Engineers of the AIME, Denver, Colo. (1977).
3. N. J. Zabusky and M. D. Kruskal, *Phys. Rev. Lett.* **15**, 240 (1965).
4. A. C. Scott, F. Y. F. Chu, D. W. McLaughlin, *Proc. IEEE* **61**, 1443 (1973).
5. J. Scott Russell, *Report on Waves* (Murray, London, 1844), pp. 311-390.
6. D. J. Korteweg and G. deVries, *Philos. Mag.* **39**, 422 (1895).
7. R. M. Miura, *SIAM (Soc. Ind. Appl. Math.) Rev.* **18**, 412 (1976).
8. M. F. Maury, *The Physical Geography of the Sea and Its Meteorology* (Harper, New York, 1861), pp. 404-405.
9. R. B. Perry and G. R. Schimke, *J. Geophys. Res.* **70**, 2319 (1965).
10. O. M. Phillips, *Annu. Rev. Fluid Mech.* **7**, 93 (1974).
11. E. C. Lafond and C. B. Rao, *Andhra Univ. Mem. Oceanogr.* **1**, 102 (1954).
12. C. S. Gardner, J. M. Green, M. D. Kruskal, R. M. Miura, *Phys. Rev. Lett.* **19**, 1095 (1967).
13. H. Segur, *J. Fluid Mech.* **59**, 721 (1973).
14. J. L. Hammack and H. Segur, *ibid.* **65**, 289 (1974).

15. G. B. Whitham, *Linear and Nonlinear Waves* (Wiley, New York, 1964), pp. 577-612.
16. T. B. Benjamin, *J. Fluid Mech.* **25**, 241 (1966); *ibid.* **29**, 559 (1967).
17. H. Ono, *J. Phys. Soc. Jpn.* **39**, 1082 (1975).
18. R. J. Joseph, *J. Phys. A: Math. Gen.* **10** (No. 12), L225 (1977).
19. T. Kubota, D. R. S. Ko, L. D. Dobbs, *J. Hydro-naut.* **12**, 157 (1978).
20. H. H. Chen and Y. C. Lee, *Phys. Rev. Lett.* **43**, 264 (1979).
21. V. D. Djordjevic and L. G. Redekopp, *J. Phys. Oceanogr.* **8**, 1016 (1978).
22. O. M. Phillips, *Dynamics of the Upper Ocean* (Cambridge Univ. Press, London, 1969), p. 169.
23. J. R. Apel, H. M. Byrne, J. R. Proni; R. L. Charnell, *J. Geophys. Res.* **80**, 865 (1975); J. R. Apel, J. R. Proni, H. M. Byrne, R. L. Sellers, *Geophys. Res. Lett.* **2**, 128 (1975).
24. J. R. Apel, *NASA Spec. Publ. SP-412* (1978), vol. 2.
25. D. J. Benney, *J. Math. Phys.* **45**, 52 (1966).
26. D. Farmer and J. D. Smith, in *Hydrodynamics of Estuaries and Fjords*, J. Nihoul, Ed. (Elsevier, New York, 1978), p. 465.
27. A. E. Gargett, *Deep-Sea Res.* **23**, 17 (1976).
28. K. Hunkins and M. Fliegel, *J. Geophys. Res.* **78**, 539 (1973).
29. C.-Y. Lee and R. C. Beardsley, *ibid.* **79**, 453 (1974).
30. T. Maxworthy, *ibid.* **84**, 338 (1979).
31. R. S. Johnson, *J. Fluid Mech.* **60**, 813 (1973).
32. J. W. Miles, *ibid.* **91**, 181 (1979).
33. ———, *ibid.* **84**, 181 (1978).
34. K. Ko and H. H. Kuehl, *Phys. Fluids* **22**, 1343 (1979).
35. A. S. Peters and J. J. Stoker, *Commun. Pure Appl. Math.* **13**, 115 (1960).
36. R. I. Scarlet played a major role in the design of the program. We are indebted to S. C. Freden (NASA Goddard Space Flight Center) and A. Strong (National Environmental Satellite Service Center, National Oceanic and Atmospheric Administration) for help in accessing the LANDSAT and NIMBUS satellites, respectively. M. N. Greer graciously pointed out (8). J. R. Apel kindly brought to our attention (24) and the Apollo-Soyuz photograph of the Andaman Sea. R. L. Gordon provided valuable assistance in a previous phase of our analysis. K.-K. Tung provided stimulating conversations.

Oils and Rubber from Arid Land Plants

Jack D. Johnson and C. Wiley Hinman

Arid land vegetation has the potential to relieve some of the United States' dependency on imported oils and rubber. The development of this vegetation could bring into cultivation new cash crops on lands currently not used for food or fiber production. In this article we discuss the economic development potential of *Cucurbita* species (principal-

Cucurbita

Potential uses of *Cucurbita* species include the production of edible oil and protein by-products from the seed, industrial starch from the roots, and forage from the vines. The species most often discussed are *Cucurbita foetidissima* (buffalo gourd), *C. digitata*, *C. palmata*

Summary. In this article the economic development potentials of *Cucurbita* species (buffalo gourd and others), *Simmondsia chinensis* (jojoba), *Euphorbia lathyris* (gopher plant), and *Parthenium argentatum* (guayule) are discussed. All of these plants may become important sources of oils or rubber.

ly buffalo gourd), *Simmondsia chinensis* (jojoba), *Euphorbia lathyris* (gopher plant), and *Parthenium argentatum* (guayule). All of these plants can be grown on arid lands, that is lands that are semiarid or drier, and they may become important sources of oils or rubber (1). Included within our definition of "oils" are many edible products as well as substances that may be useful as cosmetic and lubricant bases, waxes, or chemical feedstocks or fuels.

(coyote melon), and *C. pepo*, all of which may provide good economic returns. A major effort to domesticate the buffalo gourd and to industrialize its production is being conducted by Bemis *et al.* (2) at the University of Arizona, and we report some of this work here.

The plant is perennial, reproduces asexually, grows as a weed in regions of low rainfall, and produces a large crop of seeds rich in oil and protein. The roots may weigh up to 50 kilograms after three or four seasons of growth and consist largely of starch. This starch can be hydrolyzed chemically or enzymatically to glucose (dextrose) that is used as a sweetener in foods and beverages. The

vines grow along the ground and because of their protein content [10 to 13 percent (3)] and digestibility may have forage value.

The oil of the seed has a high ratio of unsaturated to saturated fatty acids that makes it attractive for possible use in foods prepared for consumption by humans. Linoleic acid, an essential fatty acid in the diet of humans and animals, is present in amounts ranging from 50 to 60 percent. Incorporation of the crude oil into the diet of weanling mice in amounts up to 11 percent of the total diet produced excellent growth with no evidence of deleterious effects (2).

The crude oil can be extracted from the seed by a solvent process or by mechanical pressing. The remaining seed meal, which contains about 45 percent protein and 45 percent fiber, may be used in raw form as a component of animal feeds. Studies with rodents show that the protein quality of seed meal from the buffalo gourd is similar to that of soybean and cottonseed meals.

Analysis of whole seeds indicates the presence of 32.9 percent crude protein and 33.0 percent crude fat (2). Hoffmann (4) obtained a whole-seed cyclohexane extract of 16.5 percent. The cyclohexane extract is indicative of relatively high caloric yield and high hydrocarbon content. With seed yields of up to 3000 kilograms per hectare and an estimated 16 percent hydrocarbon content, about 3.5 barrels of crude oil could be produced per hectare. Thus the buffalo gourd is not particularly promising as a producer of crude oils for hydrocarbon use. However, with 1 hectare of this crop producing 1 ton of vegetable oil and 0.5 ton of protein being produced from the seeds, the potential crop value is \$650 per hectare. This is based on a value of \$0.55 per kilogram of vegetable oil and \$0.20 per kilogram of crude protein. Since an estimated 13.5 tons of crude starch per hectare could be produced every 3 years, the approximate value of the starch

J. D. Johnson is director of the Office of Arid Lands Studies, University of Arizona, Tucson 85719, and C. W. Hinman is director of Exploratory Technology, Diamond Shamrock Corporation, Tucson 85718.